

Article

# Investigation into the Effect of Increasing Target Temperature and the Size of Cavity Confinements on Laser-Induced Plasmas

Hongbing Yao <sup>1</sup>, Emmanuel Asamoah <sup>2,\*</sup> , Pengyu Wei <sup>3,\*</sup>, Jiawei Cong <sup>2</sup>, Lin Zhang <sup>1</sup>, James Kwasi Quaisie <sup>2</sup>, Anita Asamoah <sup>4</sup>, Kwaku Ayepah <sup>2</sup> and Weihua Zhu <sup>1,\*</sup>

<sup>1</sup> College of Science, Hohai University, Nanjing 210098, Jiangsu, China; alenyao@hhu.edu.cn (H.Y.); nuaazhangl@126.com (L.Z.)

<sup>2</sup> School of Mechanical Engineering, Jiangsu University, Zhenjiang 212013, Jiangsu, China; roycia@163.com (J.C.); jameskwasiquaisie@yahoo.com (J.K.Q.); kayepah5@icloud.com (K.A.)

<sup>3</sup> China Ship Scientific Research Center, Structural performance laboratory, Wuxi 214082, Jiangsu, China

<sup>4</sup> School of Material Science, Jiangsu University of Science and Technology, Zhenjiang 212003, Jiangsu, China; aasamoah42@yahoo.com

\* Correspondence: asamoah\_grace@hotmail.com (E.A.); wei\_pengyu@163.com (P.W.); weihua\_zhu@126.com (W.Z.); Tel.: +86-15-6061-06057 (E.A.); +86-05-1085-55193 (P.W.); +86-02-8378-6626 (W.Z.)

Received: 27 February 2020; Accepted: 17 March 2020; Published: 19 March 2020



**Abstract:** In this work, the effect of the sample temperature on the magnesium (Mg) and titanium (Ti) plasmas generated by a Q-switched Neodymium-doped Yttrium Aluminum Garnet (Nd:YAG) laser operating at its fundamental wavelength of 1064 nm has been investigated. We observed that increasing the sample temperature significantly enhanced the emission intensities of the plasmas. Comparing the emission peak intensities of the case of 100 °C to the case of 300 °C, we recorded a substantial enhancement of the peak intensities of the latter compared to the former. From these results it can be observed that increasing the sample temperature has a significant effect on the emission intensities of the plasmas. We also studied the plasma dynamics and found that increasing the sample temperature also decreases the air density around the Mg sample surface. The reduction in the air density resulted in a decrease in the radiation process and lowers collision probability. Furthermore, as the plasma expands, the plasma pressure also decreases. In addition, we also employed circular and square cavities to confine the titanium plasma, and investigated the effect of the sizes of the circular and square cavities on the titanium plasma. We observed a general improvement in the emission intensities with both the circular and square cavities and attributed this improvement to the plasma compression effect of the shock waves produced by the plasma within the cavities.

**Keywords:** LIBS; electron temperature; electron density; Ti-alloy; Mg-alloy; cavity confinement

## 1. Introduction

Laser induced breakdown spectroscopy (LIBS) has been utilized in various fields such as forensics [1–3], pharmaceuticals [4], military and security [5,6], environmental analysis [7–9], archeological analyses [10–12] and material processes to analyze the target samples both qualitatively and quantitatively [13–16]. In recent decades, the field of laser induced breakdown spectroscopy has gained great attention from scientists from the fields of material sciences, plasma physics and analytical chemistry [17–19] all over the world due to its numerous applications in analyzing the elemental compositions of samples from solids [20], liquids [21] and gasses [22–25]. LIBS offers numerous advantages when compared to other similar techniques such as mass spectroscopy, the electrode spark

and the inductively coupled plasma [26]. The distinctive feature of this analytical technique is that it is a non-destructive technique, because it uses an infinitesimal amount of the target material for the analysis [27]. It also requires no sample preparation, has remote sensing capability [28] and it is a viable technique for in-situ measurements [21,29–31]. This technique uses a highly energetic laser pulse focused on the surface of the target material to generate a plasma plume on the surface of the target material. The emitted radiation is collected by the fiber bundle through the spectrometer to analyze the elemental compositions of the samples. For LIBS analysis, the produced plasma should be optically thin and the condition of local thermodynamic equilibrium (LTE) should be established [27].

The analytical performance of the plasma largely depends on numerous laser parameters such as: the wavelength, pulse duration, pulse repetition rate and laser fluence [32]. In LIBS the nature of the ambient environment can also influence the plasma expansion and the plasma properties such as electron temperature and electron density [33–37].

Several papers have been published, which document the research that has already been conducted on the laser-induced breakdown spectroscopy with cavity confinement and increasing sample temperatures.

Guo et al. [38] investigated the effect of the sample temperature of a laser-induced brass plasma. They compared the spectral intensity recorded under 25 and 200 °C sample temperature. They found that the spectral intensity of the case of 200 °C was higher than that of 25 °C. They also reported the time-resolved plasma temperatures at different sample temperatures of 25, 100 and 200 °C with laser energies of 15.5 and 24.8 mJ. Their results shows that the excitation temperature for the case of higher sample temperature is higher than that with lower sample temperature. They further studied the electron densities, and they observed a decrease in the electron density with increasing delay time. They also recorded a rapid increase in the plasma plume with increasing delay time. They observed that as the size of the plasma increases, the electron density significantly drops. They concluded that the rapid decay in the electron density under higher sample temperature is faster than the case of lower sample temperature.

Ren et al. [39] studied the characteristics of laser-induced plasma spectroscopy using cavity confinement and Au-nanoparticles. Their results show that the greatest spectral line enhancement was recorded with cavity confinement of 5 mm diameter. By combining the NELIBS with the cavity confinement, the spectral intensity of the plasma was significantly enhanced with a factor of 20.24 for the CuI 515.4 nm spectral line. They also recorded the maximum signal-to-noise ratio (SNR) of 337.1 with a pulse energy of 60 mJ under a combination of NELIBS and the cavity confinement.

In this paper, we investigated the influence of sample temperature on the spectra intensities of Mg and Ti laser-induced plasmas produced by a Q-switched Nd:YAG laser with a fundamental wavelength of 1064 nm at atmospheric pressure. We also studied the effect of the sizes of the cavity confinements on spectral intensity of the Ti plasma under several delay times and different laser fluences.

## 2. Experimental Setup and Procedure

The experimental setup of the laser-induced breakdown spectroscopy used for the study of the cavity confinement is shown in Figure 1a. We employed a Q-switched Nd:YAG laser system operating at its fundamental wavelength of 1064 nm to produce the plasma. The repetition rate of the laser was 10 Hz, and a pulse duration was 10 ns. The laser was focused to a spot size of approximately 0.42 mm in diameter on the target sample by a plano-convex lens with a focal length of 15 cm. A pyrometric detector (Ophir Optronics Solutions Ltd., energy sensor, L50 (300) A-LP2-65, P/N 7Z02782, Jerusalem, Israel) was used to measure the three different laser fluences used in this experiment (12.9, 18.1 and 23.3 J cm<sup>-2</sup>). The samples used in this investigation were titanium and magnesium alloys with percentage purity of 99.98% and 99.99%, respectively. We used two different cavities with three different diameters and three different sides, circular and square cavities, respectively. The depth of all the cavities were 7 mm. The target samples were mounted on a 3D translation stage, and the cavities were tightly fixed on the surface of the target samples. The plasma was generated in the exact center of

the cavity. The light emitted by the plasma was captured by the light collector through an optical fiber (50  $\mu\text{m}$  core diameter) which was connected to echelle spectrometer (Andor Tech., Mechelle 5000. Wavelength range of 200–975 nm, wavelength accuracy of  $\pm 0.05$  nm, focal length of 195 mm and high resolution power up to 6000 and with spectral resolution of  $\lambda/\Delta\lambda = 5000$ ) with an inbuilt intensified charge-coupled device (ICCD) camera ( $1024 \times 1024$  pixels iStar DH-334T from Andor Technology). The delay generator (Stanford Research System, model DG645, Carlsbad, CA, USA) was synchronized with the ICCD to delay the time between the laser pulses, the photodiode was used to trigger the ICCD, and the signals were monitored by the digital oscilloscope (YOKOGAWA, digital oscilloscope DL9140, Tokyo, Japan). The spectra data was an average of 15 laser shots. The experiment was conducted in air at atmospheric pressure.

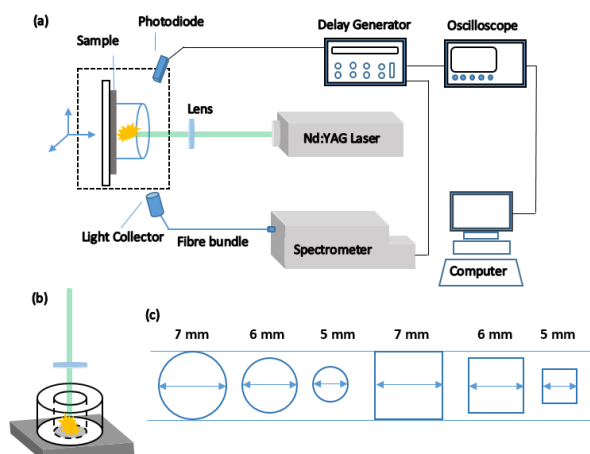


**Figure 1.** (a) The schematic diagram of the cavity confinement of the laser-induced plasma, (b) the image of the circular cavity confinement, (c) the diagram shows the circular cavities with three different sizes (5, 6 and 7 mm) and square cavities of three different lengths of sides (5, 6, 7 mm) used for the confinement.

We used the schematic diagram in Figure 2 to study the spectral emission intensity of laser-induced Mg and Ti plasmas at different sample temperatures. We employed the same laser system with the same laser parameters from Figure 1a. The target samples were fixed to the surface of the heating element. The heating element consisted of two main components: a thermocouple to monitor the temperature of the sample in order to keep a consistent sample temperature throughout the experiment and a heating resistor to heat the sample when the temperature of the sample dropped below the desired temperature. We also utilized the same focusing lens, optical fiber and echelle spectrometer used in Figure 1a. The optical signals of the plasma were collected via the optical fiber coupled to the echelle spectrometer and the spectrum obtained was analyzed using the manufacturers' software (Andor Solis (i) software, Andor Technology, Oxford Instruments Company, Munich, Germany).

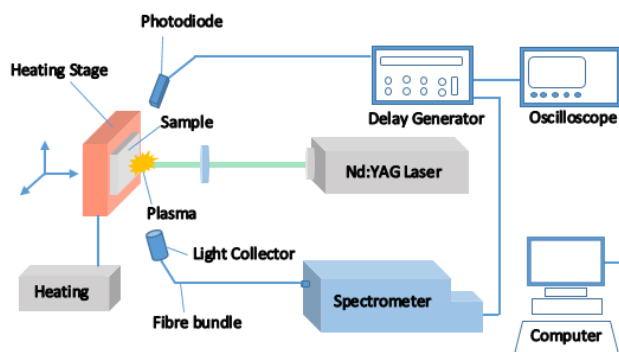


**Figure 2.** Schematic diagram of the setup used for the target heating of the samples.

### 3. Results and Discussion

#### 3.1. Effect of Target Temperature

##### 3.1.1. Emission Intensity

We recorded the emission spectra of the Mg and Ti lines at a laser fluence of  $12.9 \text{ J cm}^{-2}$  and delay time of  $12 \mu\text{s}$  in air at atmospheric pressure with and without sample heating. We compared the Mg I-518.3 nm spectral line for the case of sample temperature of  $100 \text{ }^\circ\text{C}$  to the one without the sample heating and their emission intensities were recorded as 8934 and 6140, respectively, with an enhancement factor of 1.46. From this we observed that the emission spectra of the Mg lines were more enhanced with a sample temperature of  $100 \text{ }^\circ\text{C}$  than the spectra without sample heating as shown in Figure 3a. In addition, the Ti spectra with a sample temperature of  $100 \text{ }^\circ\text{C}$  and that without sample heating are presented in Figure 3b. By comparing the Ti II-376.0 nm spectral line of the case of  $100 \text{ }^\circ\text{C}$  sample heating to the one without sample heating. The emission intensities of the Ti II-376.0 nm spectral line were recorded as 4535 and 3079 for the  $100 \text{ }^\circ\text{C}$  sample heating and the one without sample heating, respectively. The Ti spectra recorded an enhancement in the spectral intensity with sample temperature of  $100 \text{ }^\circ\text{C}$ .

In order to further analyze the Ti spectra in Figure 3b we compared the Ti spectral lines with four different spectral regions ranging from 330–340 nm, 365–377 nm, 427–448 nm and 447–460 nm as presented in Figure 4 and we found out that the Ti spectra with sample temperature of  $100 \text{ }^\circ\text{C}$  were improved within all the spectral regions.

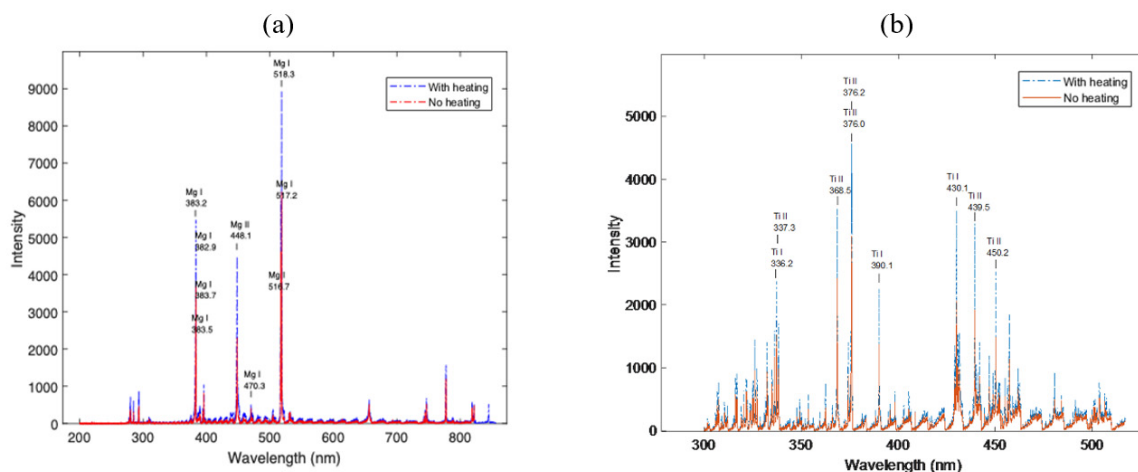


**Figure 3.** (a) Laser induced breakdown spectroscopy (LIBS) spectra of Mg plasma with sample temperature of  $100 \text{ }^\circ\text{C}$  and with no sample heating at a delay time of  $12 \mu\text{s}$  and laser fluence of  $12.9 \text{ J cm}^{-2}$ . (b) LIBS spectra of Ti plasma with sample temperature of  $100 \text{ }^\circ\text{C}$  and with no sample heating at a delay time of  $12 \mu\text{s}$  and laser fluence of  $12.9 \text{ J cm}^{-2}$ .

To better investigate the effect of increasing sample temperature on the Mg and Ti plasmas we studied the emission spectra by varying the sample temperatures from  $50$  to  $300 \text{ }^\circ\text{C}$ . Figure 5a presents the graph of the temperature dependence of Mg I-518.4 nm spectral line for three different laser fluences ( $12.9$ ,  $18.1$  and  $23.3 \text{ J cm}^{-2}$ ). The figure reveals that the spectral intensities of the Mg lines increase with an increasing sample temperature from  $50$  to  $300 \text{ }^\circ\text{C}$ . We observed that at the laser fluence of  $23.3 \text{ J cm}^{-2}$ , the emission intensity was more improved when compared with the laser fluences of  $12.9$  and  $18.1 \text{ J cm}^{-2}$ . Furthermore we found that increasing the laser fluence also improved the emission intensities of the Mg spectra.

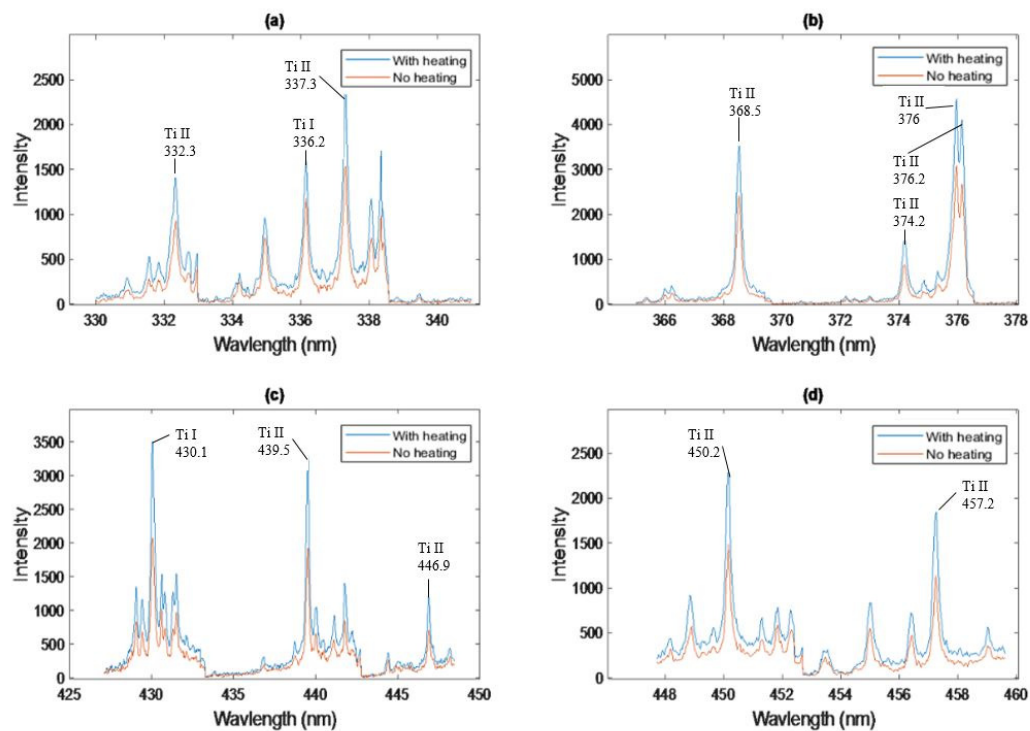


**Figure 4.** LIBS spectra of the Ti plasma with four different spectral regions with sample temperature of 100 °C and without sample temperature at a delay time of 12  $\mu$ s and laser fluence of 23.3 J cm<sup>-2</sup>. (a) from the spectral range of 330–340 nm; (b) from the spectral range of 365–377 nm; (c) from the spectral range of 427–448 nm; (d) from the spectral range of 447–460 nm.

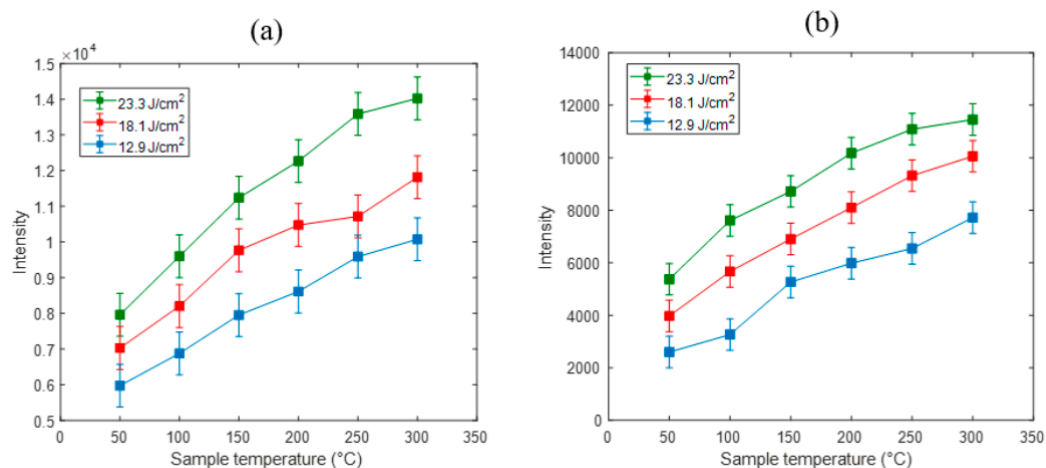


**Figure 5.** (a) Emission intensity of Mg I-518.4 nm with sample temperatures for different laser fluences at a delay time of 15  $\mu$ s. (b) Emission intensity of Ti II-376.2 nm with sample temperatures for different laser fluences at a delay time of 15  $\mu$ s.

The temperature dependence of the Ti spectra is also presented in Figure 5b. By increasing the sample temperatures, the emission spectra intensity of the Ti II-376.2 nm were increased. At a sample temperature of 50 °C the spectral intensities were recorded as 2484, 3977 and 5332 with laser fluences of 12.9, 18.1 and 23.3 J cm<sup>-2</sup>, respectively. The maximum peak intensity of the Ti II-376.2 nm lines were obtained as 11,364 with a sample temperature of 300 °C and a laser fluence of 23.3 J cm<sup>-2</sup>. By comparing the peak intensity of the lower sample temperature (50 °C) to the higher sample temperature (300 °C), we observed that the higher sample temperature (300 °C) was massively enhanced. We observed that the emission spectra of the Mg and Ti spectral lines were more enhanced using a lower laser fluence

and higher sample temperature as compared to those using a lower sample temperature and higher laser fluence.

Figure 6a depicts the temporal evolution of the Mg I-518.4 nm spectral peak intensity as a function of the delay time at different sample temperatures (100, 200 and 300 °C). As seen from Figure 6a, the peak intensities of the Mg I-518.4 nm lines recorded its maximum peak intensity as 18,101 at a delay time of 3  $\mu\text{s}$  and then drops significantly to spectral intensity of 3229 at a delay time of 30  $\mu\text{s}$ . By comparing the emission peak intensities of the case of 100 °C to the case of 300 °C we observed that the emission peak intensities of the latter were substantially more enhanced than those of the former. It can also be seen from the figure that the peak intensities of the Mg I-518.4 nm lines drop tremendously with increasing delay time.

The temporal evolution of the Ti II-376.2 nm lines is also shown in Figure 6b. The peak intensities of the Ti II-376.2 nm lines were recorded as 14,056 and 17,124 with sample temperatures of 100 and 300 °C, respectively. We found that the spectral intensity of the 300 °C sample temperature was significantly enhanced. We also observed a sharp decrease in the peak intensities by increasing the delay time. From these results we can see that increasing the sample temperature has a massive effect on the emission intensities of the plasmas.

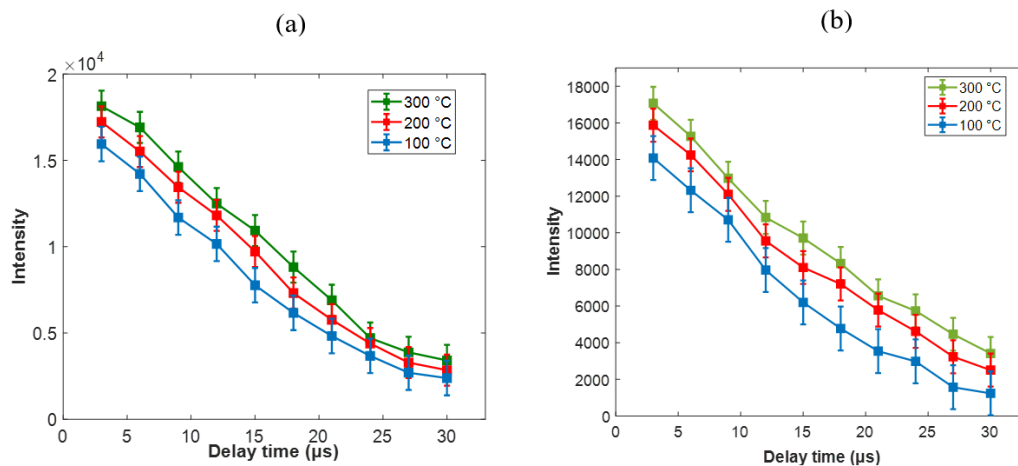


**Figure 6.** (a) Time-resolved emission line of Mg I-518.4 nm for different sample temperatures of 100, 200 and 300 °C at laser fluence of  $18.1 \text{ J cm}^{-2}$ . (b) Time-resolved emission line of Ti II-376.2 nm for different sample temperatures of 100, 200 and 300 °C at laser fluence of  $18.1 \text{ J cm}^{-2}$ .

### 3.1.2. Plasma Dynamics

Figure 7 represents the images of the plasma plume of the Mg sample acquired by a camera at different sample temperatures and laser fluences of 12.9, 18.1 and  $23.3 \text{ J cm}^{-2}$ . Increasing the sample temperature also increases the size of the plasma plume. With the same laser fluence, the size of the plasma plume increases with higher sample temperatures than that of lower sample temperatures. In addition, when the air around the Mg sample surface is heated, it causes a hydrodynamic effect, which decreases the air density near the surface of the Mg sample. Therefore, increasing the laser fluence also improves the plasma plume expansion of the generated plasma. Moreover, when the sample temperature increased, the air density surrounding the Mg sample surface reduced. The decrease in the air density resulted in a decrease in the radiation process and lower collision probability. Furthermore, as the plasma expands, the plasma pressure also decreases [40–43]. From Figure 7 we observed that the higher sample temperature lead to a substantial change in the plasma dynamics. Therefore, the Mg plasma plume expanded more with the sample temperature of 300 °C than that of the 100 and 200 °C sample temperatures. We found that the size of the Mg plasma plume had a linear relationship with the sample temperatures. Likewise, the plume expansion increases with higher laser fluence.

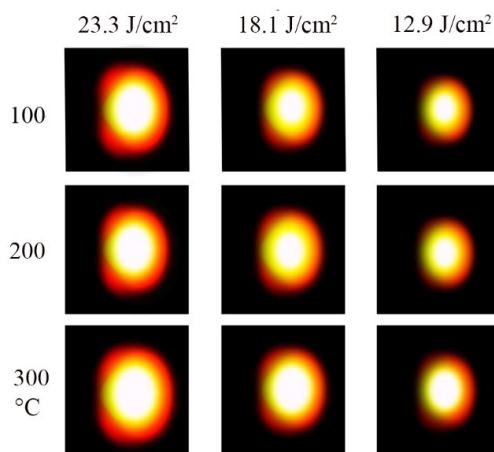


**Figure 7.** Images of the plasma plume at different laser fluences and different sample temperatures.

### 3.1.3. Electron Temperature

The electron temperature was estimated from the Boltzmann and Saha–Boltzmann plot methods by utilizing the relative intensities of the emission lines of the Mg and Ti plasmas, respectively. The plasma obtained was optically thin, and the condition for local thermodynamic equilibrium to exist was warranted [44,45].

The Boltzmann's equation can be expressed as:

$$\ln\left(\frac{\lambda_{nm}I_{nm}}{g_{nm}A_{nm}}\right) = -\frac{E_m}{k_B T_e} + \ln\left(\frac{hcN_0}{Z_0(T)}\right) \quad (1)$$

where  $g_{nm}$  and  $A_{nm}$  are statistical weight and transition probability while  $\lambda_{nm}$ ,  $I_{nm}$  and  $E_m$  are wavelength, intensity and energy of the upper state, respectively.  $N_0$  and  $h$  are the number density and Planck's constant.  $c$  and  $Z_0(T)$  are the speed of light and partition function respectively.  $k_B$  and  $T_e$  are the Boltzmann's constant and the electron temperature. The plot of Equation (1) yields a linear graph of the form  $y = mx + c$ , where  $c$  is a constant,  $y = \ln\left(\frac{\lambda_{nm}I_{nm}}{g_{nm}A_{nm}}\right)$ ,  $x = E_m$  and the slope  $m = \frac{1}{k_B T_e}$ . The relevant spectroscopic data for the Mg and Ti lines are retrieved from the NIST database [46]. The Boltzmann plot was obtained by using the spectral lines of Mg I 383.2, 470.3 and 518.4 nm spectral lines. Figure 8 depicts the Boltzmann and Saha–Boltzmann plot of the Mg and Ti spectral lines, respectively.

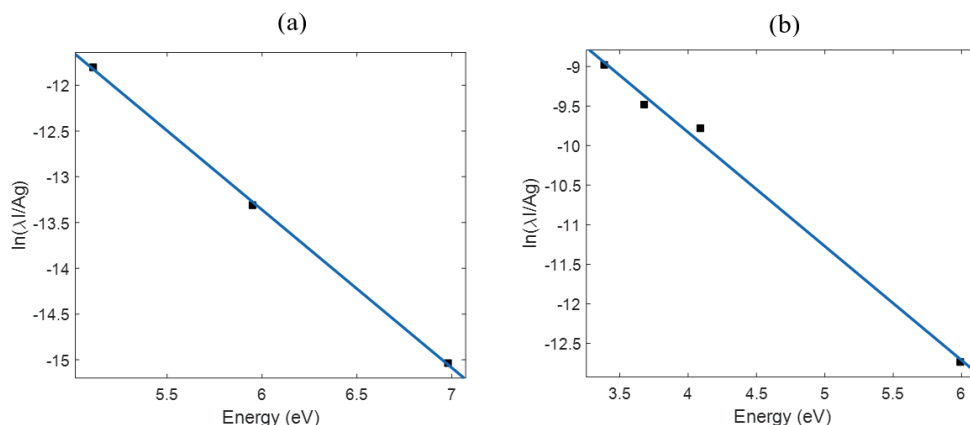


**Figure 8.** (a) The Boltzmann plot obtained from the Mg lines with a laser fluence of  $12.9 \text{ J cm}^{-2}$  without sample heating. (b) the Saha–Boltzmann plot of the Ti lines with a laser fluence of  $12.9 \text{ J cm}^{-2}$  without sample heating.

The Saha–Boltzmann equation was used to calculate the electron temperature of the Ti plasma. Equations (2) and (3) represent the ionic and neutral lines, respectively.

$$\ln\left(\frac{I_2\lambda_2}{g_2A_2}\right) - \ln\left(\frac{2(2\pi mk)(3/2)T^{3/2}}{h^3} \frac{1}{N_e}\right) = -\frac{1}{k_B T_e}(E_k^2 + E_{IP}) + \ln\left(hc \frac{N_0}{Z_0(T)}\right) \quad (2)$$

$$\ln\left(\frac{\lambda_1 I_1}{g_1 A_1}\right) = -\frac{E_k^1}{k_B T_e} + \ln\left(\frac{hc N_0}{Z_0(T)}\right) \quad (3)$$

The expression in Equation (2) can be condensed into the form of the Boltzmann's equation in Equation (1). Where  $E_{IP}$  is the ionization energy,  $m$  is the mass of the electron, and the subscripts 1 and 2 denotes the neutral and ionic lines, respectively [44,47–50].

For the case with a sample temperature of 300 °C and a laser fluence of 23.3 J cm<sup>-2</sup> the electron temperature of the Mg plasma was calculated to be 17,573 K. In addition, the electron temperature for the case without sample temperature was found to be 14,258 K at a laser fluence of 23.3 J cm<sup>-2</sup>. Comparing the electron temperatures of the case with sample temperatures with that without sample temperatures, we found that the electron temperatures of the case with sample temperatures were more enhanced as compared with the case without sample temperature.

#### 3.1.4. Electron Density

The electron density can be estimated by the Stark broadening method. The Mg I–518.4 nm and Ti II–376.2 nm spectral lines were used to deduce the electron density of the Mg and Ti plasmas, respectively from the profile of the Stark broadening lines. The electron-impact parameter can be deduced from the expression [16,50]:

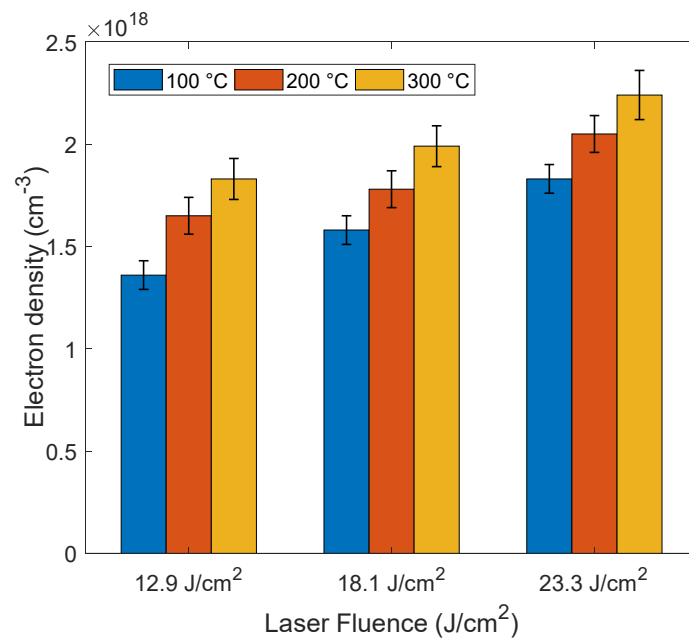
$$\Delta\lambda_{1/2}(nm) = 2\omega\left(\frac{N_e}{10^{16}}\right) + 3.5A\left(\frac{N_e}{10^{16}}\right)^{1/4} \times \left[1 - \frac{3}{4}N_D^{-1/3}\right] \omega\left(\frac{N_e}{10^{16}}\right) \quad (4)$$

where  $N_D$  is the number density in a Debye sphere,  $\Delta\lambda_{1/2}$  is the full width at half maximum (FWHM).  $A$ ,  $N_e$  and  $\omega$  are the ionic-impact broadening parameter, the electron density and the electron-impact parameter, respectively. If we do not consider the contribution of the ionic broadening, the Equation (4) can then be expressed in the form:

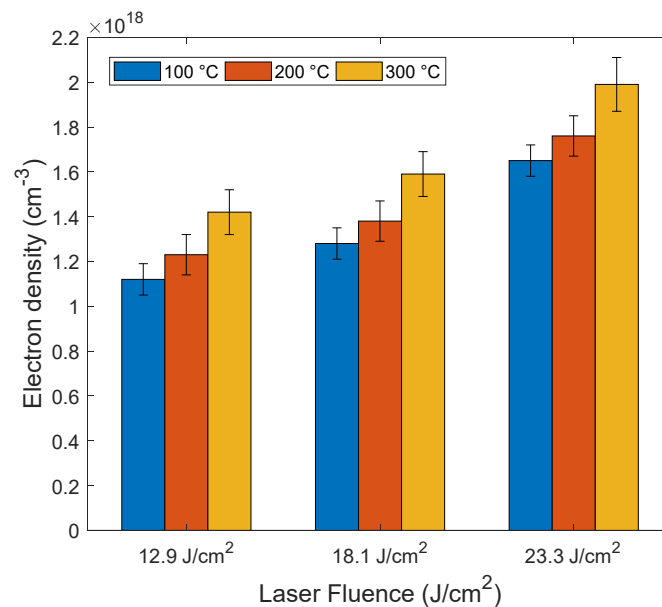
$$\Delta\lambda_{1/2}(nm) = 2\omega\left(\frac{N_e}{10^{16}}\right) \quad (5)$$

Figure 9 presents the electron density of the Mg plasma as a function of laser fluence at different sample temperatures (100, 200 and 300 °C) at a delay time of 3 μs. The maximum value of the electron density was obtained as 2.24 × 10<sup>18</sup> cm<sup>-3</sup> with a sample temperature of 300 °C at a laser fluence of 23.3 J cm<sup>-2</sup>. From this graph it can be seen that the electron density drops with higher laser fluences.

Figure 10 also shows the electron density of the Ti plasma with different sample temperatures. It can be seen that the electron density significantly drops with increasing sample temperature. With the sample temperatures of 100, 200 and 300 °C the electron density was found to be 1.65 × 10<sup>18</sup>, 1.76 × 10<sup>18</sup> and 1.99 × 10<sup>18</sup> cm<sup>-3</sup> respectively at a laser fluence of 23.3 J cm<sup>-2</sup>. By comparing the electron density of the case of 300 °C sample temperature to that without the sample temperature, we found that the electron density of the case of 300 °C sample temperature was more enhanced. We also observed that the electron densities drop rapidly with increasing laser fluence.



**Figure 9.** Electron density of the Mg plasma as a function of laser fluence of at different sample temperatures.



**Figure 10.** Electron density of the Ti plasma as a function of laser fluence at different sample temperatures.

### 3.2. Effect of the Cavity Confinements

#### 3.2.1. Emission Intensity

The spectral intensity of the plasma can be improved by the cavity confinements, while the performance of the cavity confinement itself is influenced by different factors such as its size, laser fluence and the wavelength. The size of the confinement plays a vital role in the plasma enhancement because of the plasma compression effect of the shock waves produced by the plasma within the cavity. Throughout this experiment we employed circular and square cavities with three different sizes and investigated the effect of the sizes on the laser-induced Ti plasma. Figure 11 shows the spectral peak intensities of the Ti plasma confined with three different sizes of the circular cavity. We observed that the circular cavity with the 5 mm diameter produced the greatest spectral peak intensity of the Ti

II–318.2 nm spectral lines. By comparing the spectral intensities of the confinement of the circular cavity with 5 mm diameter to the one without confinement, it was found that the spectral intensity of the former was significantly enhanced with an enhancement factor of 1.76. We attributed these signal enhancements to the compression effect of the shock wave. In addition, by comparing the three circular cavity sizes as seen from Figure 11, we found that the 5 mm diameter cavity had the best enhancement. From our results we observed that the smaller cavity size had the higher spectral intensity enhancement. As the plasma cools down, the spectral intensities of the lines then drops with time [51,52]. From the time-resolved emission intensities in Figure 11, we observed that the line intensities of the Ti II–318.2 nm decays exponentially with increasing delay time.

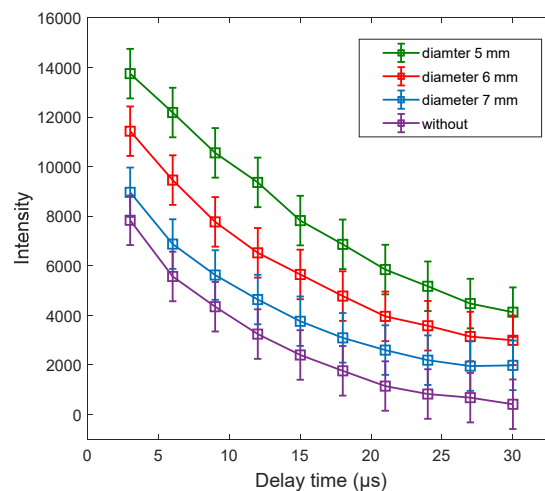


**Figure 11.** Time-resolved emission intensities of the Ti II–318.2 nm spectral lines for different sizes of the circular cavity at laser fluence of  $18.1 \text{ J cm}^{-2}$ .

Figure 12 also depicts the time-resolved emission intensities of the Ti plasma confined with different sizes of the square cavities with 5, 6 and 7 mm length of side. We observed a drop in the spectral intensities with increasing delay time. By comparing the square cavity confinements to the case without confinement we recorded a tremendous increase of the spectral intensities with the square cavity confinements. At a delay time of  $3 \mu\text{s}$  and a laser fluence of  $18.1 \text{ J cm}^{-2}$  we found that the square cavity with a 5 mm length of side produced the maximum spectral peak intensity with an enhancement factor of 2.15.

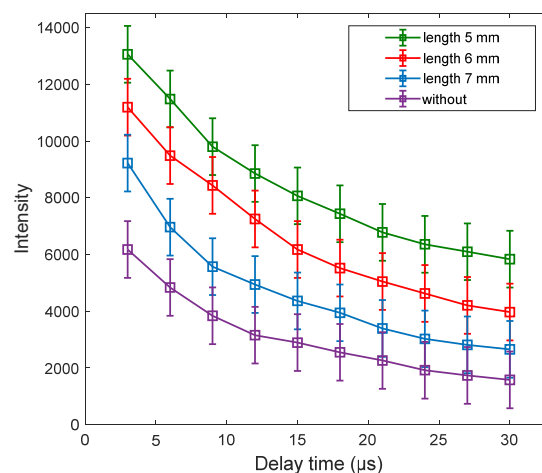


**Figure 12.** Time-resolved emission intensities of the Ti II–318.2 nm spectral lines for different sizes of the square cavity at laser fluence of  $18.1 \text{ J cm}^{-2}$ .

### 3.2.2. Electron Temperature

The electron temperature of the Ti plasma confined in circular and square cavities was deduced from the Saha–Boltzmann’s equation. The electron temperature was calculated from the slope of the linear plot for the Ti plasma. For the case without the cavity confinement the electron temperature was found to be 8546 K with a laser fluence of  $12.9 \text{ J cm}^{-2}$ . After employing a circular cavity with a 5 mm diameter, we recorded the electron temperature to be 12,546 K with a laser fluence of  $12.9 \text{ J cm}^{-2}$ . Figures 13 and 14 show the plots of the electron temperature against the different sizes of the circular and square cavities respectively. From these plots we found that the electron temperature increases with higher laser fluences. We also observed that as the size of the circular and the square cavities decreased, the electron temperatures increased. Moreover, after comparing the electron temperature of the case without cavity confinement with the square cavity confinement it was found that the electron temperature of the latter was more enhanced, as seen in Figure 14.

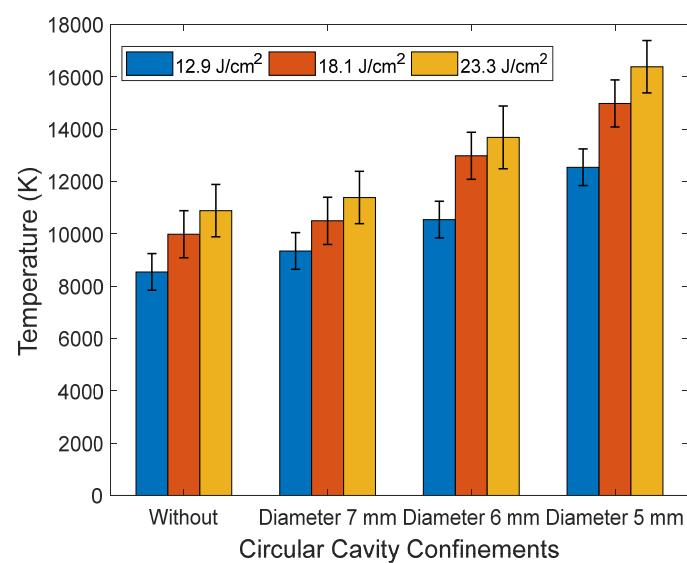


**Figure 13.** A graph of electron temperature versus the circular cavities with different sizes and without cavity confinement, at laser fluences  $12.9$ ,  $18.1$  and  $23.3 \text{ J cm}^{-2}$ .

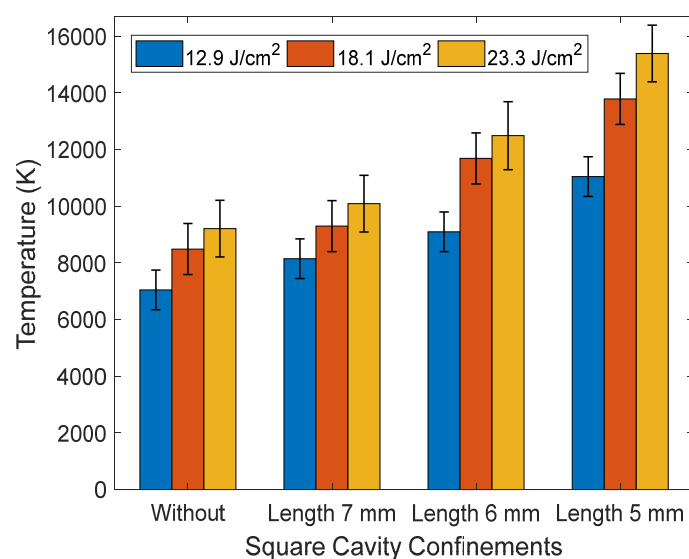


**Figure 14.** A graph of electron temperature versus the square cavities with different sizes and without cavity confinement, at laser fluences  $12.9$ ,  $18.1$  and  $23.3 \text{ J cm}^{-2}$ .

In addition, comparing the electron temperatures of the circular cavities in Figure 13 and the square cavities in Figure 14, it can be seen that the circular cavities with a 5 mm diameter had the highest electron temperature of 16,389 K.

The time-resolved electron temperatures of the Mg and Ti plasmas confined with circular cavity of different sizes at a laser fluence of  $23.3 \text{ J cm}^{-2}$  are presented in Figures 15 and 16, respectively. We observed that for the Mg plasma, the maximum electron temperature reached 17,552 K at a delay time of  $3 \mu\text{s}$ . By increasing the delay time to  $30 \mu\text{s}$  the electron temperature rapidly dropped to 7835 K. Moreover, the Ti plasma also had its maximum electron temperature of 16,509 K at a delay time of  $3 \mu\text{s}$ . As Figure 15 shows, with further increase in the delay time, the electron temperature sharply drops to its minimum electron temperature of 2786 K at  $30 \mu\text{s}$ .

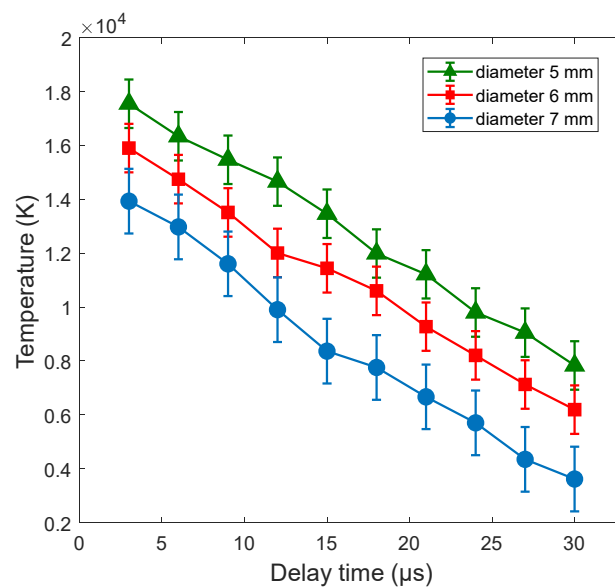


**Figure 15.** Time-resolved electron temperatures of the Ti plasma at different sizes of the circular cavity at a laser fluence of  $23.3 \text{ J cm}^{-2}$ .

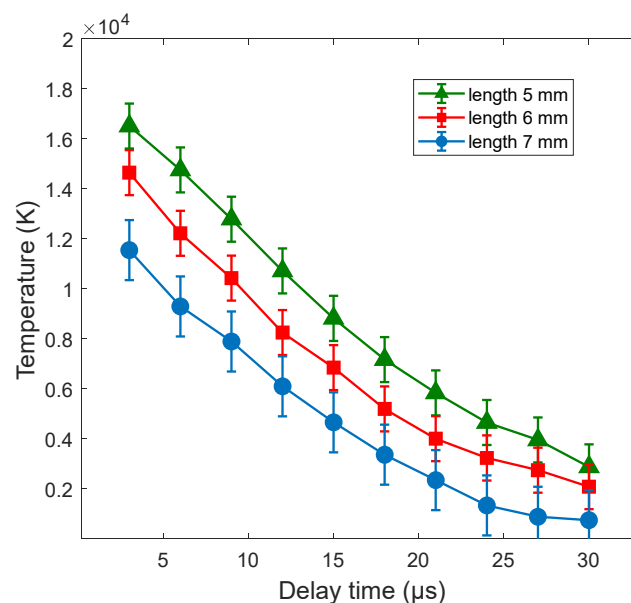


**Figure 16.** Time-resolved electron temperatures of the Ti plasma at different sizes of the circular cavity at a fluence of  $23.3 \text{ J cm}^{-2}$ .

#### 4. Conclusions

In this study, we investigated the effect of increasing the sample temperature of the laser-produced magnesium and titanium plasmas. We studied the emission spectra of the Mg and Ti plasmas by varying the sample temperatures from 50 to 300 °C while varying delay times. In this study we found that increasing the sample temperature significantly enhanced the emission intensities of the plasmas. We observed that the sample temperature enhances the interactions between the laser and the plasma, thereby, causing a plasma shielding effect. In addition, we also studied the plasma dynamics, and observed that increasing the sample temperature and laser fluence increases the plasma expansion. We further investigated the effect of different sizes for both circular and square cavities on the spectral intensities and electron temperatures of the Ti plasma. We found that there is an inverse relationship between the size of the circular and the square cavities and the emission intensities and electron temperatures. As the size of circular and square cavities decreases, the emission intensities and electron temperatures both increase.

**Author Contributions:** Formal analysis, W.Z.; investigation, E.A. and A.A.; methodology, K.A.; resources, P.W. and J.K.Q.; software, E.A.; supervision, H.Y.; validation, L.Z.; visualization, J.C.; writing—original draft, E.A. All authors have read and agreed to the published version of the manuscript.

**Funding:** National Natural Science Foundation of China: 51775253, 61505071. Fundamental Research Funds for the Central Universities: 2019B02614. China Postdoctoral Science Foundation: 2017M61172.

**Acknowledgments:** This work was supported by the National Natural Science Foundation of China (Nos. 51775253, 61505071), the Fundamental Research Funds for the Central Universities (No. 2019B02614), China Postdoctoral Science Foundation (2017M611725).

**Conflicts of Interest:** The authors declare no conflict of interest.

#### References

1. Bridge, C.M.; Powell, J.; Steele, K.L.; Sigman, M.E. Forensic comparative glass analysis by laser-induced breakdown spectroscopy. *Spectrochim. Acta Part B At. Spectrosc.* **2007**, *62*, 1419–1425. [[CrossRef](#)]
2. Rodriguez-Celis, E.M.; Gornushkin, I.B.; Heitmann, U.M.; Almirall, J.R.; Smith, B.W.; Winefordner, J.D.; Omenetto, N.; Rodriguez-Celis, E.M. Laser induced breakdown spectroscopy as a tool for discrimination of glass for forensic applications. *Anal. Bioanal. Chem.* **2008**, *391*, 1961–1968. [[CrossRef](#)]
3. Naes, B.E.; Umpierrez, S.; Ryland, S.; Barnett, C.; Almirall, J. A comparison of laser ablation inductively coupled plasma mass spectrometry, micro X-ray fluorescence spectroscopy, and laser induced breakdown spectroscopy for the discrimination of automotive glass. *Spectrochim. Acta Part B At. Spectrosc.* **2008**, *63*, 1145–1150. [[CrossRef](#)]
4. Asimellis, G.; Hamilton, S.; Giannoudakos, A.; Kompitsas, M. Controlled inert gas environment for enhanced chlorine and fluorine detection in the visible and near-infrared by laser-induced breakdown spectroscopy. *Spectrochim. Acta Part B At. Spectrosc.* **2005**, *60*, 1132–1139. [[CrossRef](#)]
5. Harmon, R.S.; DeLucia, F.C.; McManus, C.E.; McMillan, N.J.; Jenkins, T.F.; Walsh, M.E.; Miziolek, A. Laser-induced breakdown spectroscopy—An emerging chemical sensor technology for real-time field-portable, geochemical, mineralogical, and environmental applications. *Appl. Geochem.* **2006**, *21*, 730–747. [[CrossRef](#)]
6. Gottfried, J.; De Lucia, J.F.C.; Munson, C.A.; Miziolek, A.W. Strategies for residue explosives detection using laser-induced breakdown spectroscopy. *J. Anal. At. Spectrom.* **2008**, *23*, 205–216. [[CrossRef](#)]
7. Lei, W.; Motto-Ros, V.; Boueri, M.; Ma, Q.; Zhang, D.; Zheng, L.; Zeng, H.; Yu, J. Time-resolved characterization of laser-induced plasma from fresh potatoes. *Spectrochim. Acta Part B At. Spectrosc.* **2009**, *64*, 891–898. [[CrossRef](#)]
8. Boueri, M.; Motto-Ros, V.; Lei, W.-Q.; Ma, Q.-L.; Zheng, L.-J.; Zeng, H.-P.; Yu, J. Identification of polymer materials using laser-induced breakdown spectroscopy combined with artificial neural networks. *Appl. Spectrosc.* **2011**, *65*, 307–314. [[CrossRef](#)]
9. Corsi, M.; Palleschi, V.; Salvetti, A.; Tognoni, E. Calibration free laser induced plasma spectroscopy: A new method for combustion products analysis. *Clean Air* **2002**, *3*, 69–79. [[CrossRef](#)]

10. Müller, K.; Stege, H. Evaluation of the analytical potential of laser-induced breakdown spectrometry (libs) for the analysis of historical glasses. *Archaeometry* **2003**, *45*, 421–433. [[CrossRef](#)]
11. Carmona, N.; Oujja, M.; Rebollar, E.; Römich, H.; Castillejo, M. Analysis of corroded glasses by laser induced breakdown spectroscopy. *Spectrochim. Acta Part B At. Spectrosc.* **2005**, *60*, 1155–1162. [[CrossRef](#)]
12. Giakoumaki, A.; Melessanaki, K.; Anglos, D. Laser-induced breakdown spectroscopy (LIBS) in archaeological science—Applications and prospects. *Anal. Bioanal. Chem.* **2006**, *387*, 749–760. [[CrossRef](#)] [[PubMed](#)]
13. Awan, M.A.; Ahmed, S.H.; Aslam, M.R.; Qazi, I.A.; Baig, M.A. Determination of heavy metals in ambient air particulate matter using laser-induced breakdown spectroscopy. *Arab. J. Sci. Eng.* **2013**, *38*, 1655–1661. [[CrossRef](#)]
14. Markiewicz-Kęszycka, M.; Casado-Gavalda, M.P.; Cama-Moncunill, X.; Cama-Moncunill, R.; Dixit, Y.; Cullen, P.J.; Sullivan, C. Laser-induced breakdown spectroscopy (LIBS) for rapid analysis of ash, potassium and magnesium in gluten free flours. *Food Chem.* **2018**, *244*, 324–330. [[CrossRef](#)] [[PubMed](#)]
15. Li, Y.; Tian, D.; Ding, Y.; Yang, G.; Liu, K.; Wang, C.; Han, X. A review of laser-induced breakdown spectroscopy signal enhancement. *Appl. Spectrosc. Rev.* **2017**, *53*, 1–35. [[CrossRef](#)]
16. Sun, Y.-X.; Zhong, S.; Lu, Y.; Sun, X.; Ma, J.-Y.; Liu, Z. Application of LIBS in Element Analysis of Nanometer Thin Film Prepared on Silicon Basement. *Guang Pu Xue Yu Guang Pu Fen Xi = Guang Pu* **2015**, *35*, 1376–1382.
17. Neogi, A.; Thareja, R.K. Laser-produced carbon plasma expanding in vacuum, low pressure ambient gas and nonuniform magnetic field. *Phys. Plasmas* **1999**, *6*, 365–371. [[CrossRef](#)]
18. Landau, L.D.; Lifshits, E.M. *Fluid Mechanics*; Pergamon Press: London, UK, 1959. (In English)
19. Zeldovich, Y.B.; Raizer, Y.P. *Physics of Shock Waves and High Temperature Hydrodynamics Phenomena*; Academic Press: Cambridge, MA, USA, 1966.
20. Sturm, V.; Péter, L.; Noll, R. Steel analysis with laser-induced breakdown spectrometry in the vacuum ultraviolet. *Appl. Spectrosc.* **2000**, *54*, 1275–1278. [[CrossRef](#)]
21. Michel, A.P.M.; Lawrence-Snyder, M.; Angel, S.; Chave, A.D. Laser-induced breakdown spectroscopy of bulk aqueous solutions at oceanic pressures: Evaluation of key measurement parameters. *Appl. Opt.* **2007**, *46*, 2507–2515. [[CrossRef](#)]
22. Cremers, D.A.; Radziemski, L.J. Detection of chlorine and fluorine in air by laser-induced breakdown spectrometry. *Anal. Chem.* **1983**, *55*, 1252–1256. [[CrossRef](#)]
23. Radziemski, L.J.; Cremers, D.A. *Laser-Induced Plasmas and Applications*; Marcel Dekker Inc.: New York, NY, USA, 1989.
24. Lee, Y.; Song, K.; Sneddon, J. *Laser Induced Plasmas for Analytical Atomic Spectroscopy*; Wiley-VCH: New York, NY, USA, 1997.
25. Sturm, V.; Noll, R. Laser-induced breakdown spectroscopy of gas mixtures of air, CO<sub>2</sub>, N<sub>2</sub>, and C<sub>3</sub>H<sub>8</sub> for simultaneous C, H, O, and N measurement. *Appl. Opt.* **2003**, *42*, 6221–6225. [[CrossRef](#)] [[PubMed](#)]
26. Amoroso, S.; Bruzzese, R.; Spinelli, N.; Velotta, R. Characterization of laser-ablation plasmas. *J. Phys. B: At. Mol. Opt. Phys.* **1999**, *32*, 131. [[CrossRef](#)]
27. Luo, W.F.; Zhao, X.X.; Sun, Q.B.; Gao, C.X.; Tang, J.; Wang, H.J.; Zhao, W. Characteristics of the aluminum alloy plasma produced by a 1064 nm Nd:YAG laser with different irradiances. *Pramana* **2010**, *74*, 945–959. [[CrossRef](#)]
28. Mendys, A.; Kanski, M.; Farah-Sougueh, A.; Pellerin, S.; Pokrzywka, B.; Dzierzega, K. Investigation of the local thermodynamic equilibrium of laser-induced aluminum plasma by Thomson scattering technique. *Spectrochim. Acta Part B At. Spectrosc.* **2014**, *96*, 61–68. [[CrossRef](#)]
29. Sallé, B.; Lacour, J.-L.; Vors, E.; Fichet, P.; Maurice, S.; Cremers, D.A.; Wiens, R.C. Laser-induced breakdown spectroscopy for Mars surface analysis: Capabilities at stand-off distances and detection of chlorine and sulfur elements. *Spectrochim. Acta Part B At. Spectrosc.* **2004**, *59*, 1413–1422. [[CrossRef](#)]
30. Arp, Z.A.; Cremers, D.A.; Harris, R.D.; Oschwald, D.M.; Parker, G.R.; Wayne, D. Feasibility of generating a useful laser-induced breakdown spectroscopy plasma on rocks at high pressure: Preliminary study for a Venus mission. *Spectrochim. Acta Part B At. Spectrosc.* **2004**, *59*, 987–999. [[CrossRef](#)]
31. Russo, R. Laser ablation in analytical chemistry—A review. *Talanta* **2002**, *57*, 425–451. [[CrossRef](#)]
32. Brygo, F.; Dutouquet, C.; Le Guern, F.; Oltra, R.; Semerok, A.; Weulersse, J. Laser fluence, repetition rate and pulse duration effects on paint ablation. *Appl. Surf. Sci.* **2006**, *252*, 2131–2138. [[CrossRef](#)]
33. Harilal, S.S.; Bindhu, C.V.; Nampoory, V.; Vallabhan, C.P.G. Influence of ambient gas on the temperature and density of laser produced carbon plasma. *Appl. Phys. Lett.* **1998**, *72*, 167–169. [[CrossRef](#)]

34. Aguilera, J.A.; Aragón, C. A comparison of the temperatures and electron densities of laser-produced plasmas obtained in air, argon, and helium at atmospheric pressure. *Appl. Phys. A* **1999**, *69*, S475–S478. [[CrossRef](#)]
35. Löbe, A.; Vrenegor, J.; Fleige, R.; Sturm, V.; Noll, R. Laser-induced ablation of a steel sample in different ambient gases by use of collinear multiple laser pulses. *Anal. Bioanal. Chem.* **2006**, *385*, 326–332. [[CrossRef](#)] [[PubMed](#)]
36. Shaikh, N.M.; Hafeez, S.; Baig, M. Comparison of zinc and cadmium plasma parameters produced by laser-ablation. *Spectrochim. Acta Part B At. Spectrosc.* **2007**, *62*, 1311–1320. [[CrossRef](#)]
37. Bashir, S.; Farid, N.; Mahmood, K.; Rafique, M.S. Influence of ambient gas and its pressure on the laser-induced breakdown spectroscopy and the surface morphology of laser-ablated Cd. *Appl. Phys. A* **2012**, *107*, 203–212. [[CrossRef](#)]
38. Guo, K.; Chen, A.; Xu, W.; Zhang, D.; Jin, M. Effect of sample temperature on time-resolved laser-induced breakdown spectroscopy. *AIP Adv.* **2019**, *9*, 065214. [[CrossRef](#)]
39. Ren, L.; Ren, L.; Tang, H.; Sun, Y. Spectral characteristics of laser-induced plasma under the combination of Au-nanoparticles and cavity confinement. *Results Phys.* **2019**, *15*, 102798. [[CrossRef](#)]
40. Zhang, D.; Chen, A.; Wang, Q.; Wang, Y.; Qi, H.; Li, S.; Jiang, Y.; Jin, M. Influence of target temperature on H alpha line of laser-induced silicon plasma in air. *Phys. Plasmas* **2018**, *25*, 083305. [[CrossRef](#)]
41. Liu, Y.; Tong, Y.; Wang, Y.; Zhang, D.; Li, S.; Jiang, Y.; Chen, A.; Jin, M. Influence of sample temperature on the expansion dynamics of laser-induced germanium plasma. *Plasma Sci. Technol.* **2017**, *19*, 125501. [[CrossRef](#)]
42. El Sherbini, A.; Hegazy, H.; El Sherbini, T. Measurement of electron density utilizing the H $\alpha$ -line from laser produced plasma in air. *Spectrochim. Acta Part B At. Spectrosc.* **2006**, *61*, 532–539. [[CrossRef](#)]
43. Sangines, R.; Sobral, H.; Alvarez-Zauco, E. The effect of sample temperature on the emission line intensification mechanisms in orthogonal double-pulse laser induced breakdown spectroscopy. *Spectrochim. Acta Part B At. Spectrosc.* **2012**, *68*, 40–45. [[CrossRef](#)]
44. Asamoah, E.; Hongbing, Y. Influence of laser energy on the electron temperature of a laser-induced Mg plasma. *Appl. Phys. A* **2016**, *123*, 22. [[CrossRef](#)]
45. Asamoah, E.; Xia, Y.; Hongbing, Y.; Wei, P.; Jiawei, C.; Weihua, Z.; Lin, Z.; Quaisie, J.K. Influence of cavity and magnetic confinements on the signal enhancement and plasma parameters of laser-induced Mg and Ti plasmas. *Laser Part. Beams* **2020**, *38*, 61–72. [[CrossRef](#)]
46. NIST. Atomic Spectra Database. Available online: [http://Physics.nist.gov/PhysRef-Data/ASD/lines\\_form.html](http://Physics.nist.gov/PhysRef-Data/ASD/lines_form.html) (accessed on 13 December 2019).
47. Gomba, J.M.; D'Angelo, C.; Bertuccelli, D.; Bertuccelli, G. Spectroscopic characterization of laser induced breakdown in aluminium–lithium alloy samples for quantitative determination of traces. *Spectrochim. Acta Part B At. Spectrosc.* **2001**, *56*, 695–705. [[CrossRef](#)]
48. Sun, D.; Su, M.; Dong, C.; Wen, G. A comparative study of the laser induced breakdown spectroscopy in single- and collinear double-pulse laser geometry. *Plasma Sci. Technol.* **2014**, *16*, 374–379. [[CrossRef](#)]
49. Griem, H. *Principles of Plasma Spectroscopy*; Cambridge University: Cambridge, UK, 1997.
50. Hongbing, Y.; Asamoah, E.; Jiawei, C.; Dongqing, Y.; Fengxiao, Y. Comprehensive study on the electron temperature and electron density of laser-induced Mg plasma. *J. Lasers Opt. Photonics* **2018**, *5*, 2.
51. Ghezelbash, M.; Majd, A.E.; Darbani, S.M.R.; Ghasemi, A. Experimental investigation of atomic and ionic titanium lines, diatomic TiO $_y$  transition and continuum background radiation via magnetically confined LIBS. *Ceram. Int.* **2017**, *43*, 8356–8363. [[CrossRef](#)]
52. Ahmed, R.; Akthar, M.; Jabbar, A.; Umar, Z.A.; Ahmed, N.; Iqbal, J.; Baig, M.A. Signal intensity enhancement by cavity confinement of laser-produced plasma. *IEEE Trans. Plasma Sci.* **2019**, *47*, 1616–1620. [[CrossRef](#)]

